Intercalation of the (1*R*,2*S*,3*R*,4*S*)-N^6-[1-(1,2,3,4-Tetrahydro-2,3,4-trihydroxybenz[*a*]anthracenyl)]-2′-deoxyadenosyl Adduct in the N-*ras* Codon 61 Sequence: DNA Sequence Effects†

Zhijun Li, Pamela J. Tamura, Amanda S. Wilkinson, Constance M. Harris, Thomas M. Harris, and Michael P. Stone*

Department of Chemistry and Center in Molecular Toxicology, Vanderbilt University, Nashville, Tennessee 37235

Received December 7, 2000; Revised Manuscript Received March 20, 2001

ABSTRACT: The structure of the bay region (1*R*,2*S*,3*R*,4*S*)-N^6-[1-(1,2,3,4-tetrahydro-2,3,4-trihydroxybenz-[*a*]anthracenyl)]-2′-deoxyadenosyl adduct at X^7 of 5′-d(CGGACAXGAAG)-3′•5′-d(CTTCTTGTCCG)-3′, incorporating codons 60, 61 (underlined), and 62 of the human N-*ras* protooncogene, was determined by NMR. This was the bay region benz[*a*]anthracene RSRS (61,3) adduct. The BA moiety intercalated above the 5′-face of the modified base pair. NOE connectivities between imino protons were disrupted at T^{16} and T^{17}. Large chemical shifts at the lesion site were consistent with ring current shielding arising from the BA moiety. A large chemical shift dispersion was observed for the BA aromatic protons. An increased rise of 8.17 Å was observed between base pairs A^6•T^{17} and X^7•T^{16}. The PAH moiety stacked with the purine ring of A^6, the 5′-neighbor nucleotide. This resulted in buckling of the 5′-neighbor A^6•T^{17} base pair, evidenced by exchange broadening for the T^{17} imino resonance. It also interrupted sequential NOE connectivities between nucleotides C^5 and A^6. The A^6 deoxyribose ring showed an increased percentage of the C3′-endo conformation. This differed from the bay region BA RSRS (61,2) adduct, in which the lesion was located at position X^6 [Li, Z., Mao, H., Kim, H.-Y., Tamura, P. J., Harris, C. M., Harris, T. M., and Stone, M. P. (1999) *Biochemistry 38*, 2969−2981], but was similar to the benzo[*a*]-pyrene BP SRSR (61,3) adduct [Zegar I. S., Chary, P., Jabil, R. J., Tamura, P. J., Johansen, T. N., Lloyd, R. S., Harris, C. M., Harris, T. M., and Stone, M. P. (1998) *Biochemistry 37*, 16516−16528]. The altered sugar pseudorotation at A^6 appears to be common to both bay region BA RSRS (61,3) and BP SRSR (61,3) adducts. It could not be discerned if the C3′-endo conformation at A^6 in the BA RSRS (61,3) adduct altered base pairing geometry at X^7•T^{16}, as compared to the C2′-endo conformation. The structural studies suggest that the mutational spectrum of this adduct may be more complex than that of the BA RSRS (61,2) adduct.

Benz[*a*]anthracene (BA)[1] is a component of coal tar, atmospheric pollution (*1*, *2*), automobile exhaust, and cigarette smoke (*3*). The toxic effects of polycyclic aromatic hydrocarbons (PAH) such as BA have been recognized since Percival Pott's linkage between the incidence of scrotal cancer in chimney sweeps and occupational exposure to soot in the 18th century (*4*). PAH genotoxicity is generally recognized to result from stepwise oxidation by cytochromes P_{450} (*5*, *6*) to stereoisomeric "bay region" electrophilic diol epoxides.

The epoxides react with nucleophilic sites on the bases of DNA, especially guanine N^2 (*7*−*9*), but also other sites, including adenine N^6 (*10*, *11*). PAH adducts at adenine N^6 are generally of lower abundance, as compared to the corresponding guanine N^2 adducts. These adducts are nevertheless of interest, as the adenine lesions may have disproportionate biological significance (*12*−*14*). Wei et al. (*15*, *16*) showed that treatment of hamster V79 cells with low doses of the tumorigenic (+)-RSSR benzo[*a*]pyrene DE-2 epoxide resulted in an increase in the proportions of mutations at adenine.

Benz[*a*]anthracene is somewhat less carcinogenic than benzo[*a*]pyrene (BP) or dibenz[*a*,*h*]anthracene (*17*, *18*). This may be due in part to a lower level of metabolism to the bay region diol epoxide (*19*−*21*). Of the stereoisomeric bay region BA diol epoxides, (*1R*,*2S*,*3S*,*4R*)-3,4-dihydroxy-1,2-

† This work was supported by NIH Grant ES-05355. Funding for the NMR spectrometer was supplied by NIH Grant RR-05805 and the Vanderbilt Center in Molecular Toxicology, ES-00267. The National Magnetic Resonance Facility at Madison was funded by the University of Wisconsin, NSF Grants DMB-8415048 and BIR-9214394, NIH Grants RR-02301, RR-02781, and RR-08438, and the USDA.

* To whom correspondence should be addressed: (615) 322-2589 (phone); (615) 343-1234 (fax); stone@toxicology.mc.vanderbilt.edu.

[1] Abbreviations: BADE, benz[*a*]anthracene diol epoxide; BPDE, benzo[*a*]pyrene diol epoxide; EDTA, ethylenediaminetetraacetic acid; HPLC, high-pressure liquid chromatography; NOE, nuclear Overhauser enhancement; NOESY, two-dimensional NOE spectroscopy; ROESY rotating-frame Overhauser enhancement spectroscopy; ppm, parts per million; TPPI, time-proportional phase increment; 1D, one dimensional; 2D, two dimensional. A right superscript refers to the numerical position in the sequence starting from the 5′-terminus of chain A and proceeding to the 3′-terminus of chain A and then from the 5′-terminus of chain B to the 3′-terminus of chain B. C2, C5, C6, C8, C1′, C2′, C2″, etc. represent specific carbon nuclei. H2, H5, H6, H8, H1′, H2′, H2″, etc. represent protons attached to these carbons.

10.1021/bi002785r CCC: $20.00
Published on Web 05/18/2001

Chart 1: (A) BA RSRS (61,3) Oligodeoxynucleotide, Where X = (1*R*,2*S*,3*R*,4*S*)-*N*^{6}-[1-(1,2,3,4-Tetrahydrobenz[*a*]anthracenyl)]-2′-deoxyadenosyl Adduct (Bottom), and (B) (1*R*,2*S*,3*R*,4*S*)-*N*^{6}-[1-(1,2,3,4-Tetrahydrobenz[*a*]anthracenyl)]-2′-deoxyadenosyl Adduct and Designations of the Benz[*a*]anthracene Protons

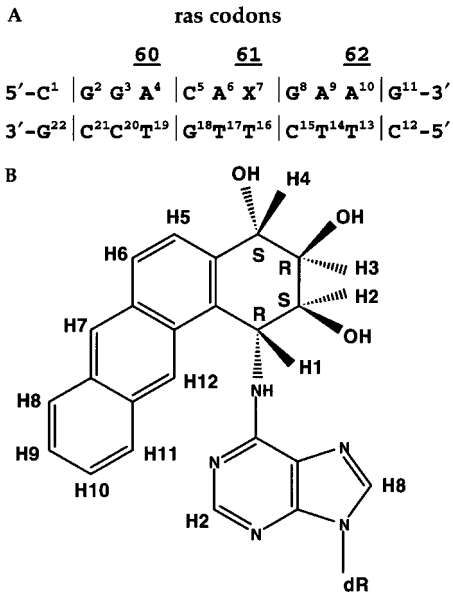

epoxy-1,2,3,4-tetrahydrobenz[*a*]anthracene (DE2) has tumor-initiating activity in mouse skin and newborn mice (*22*). This diol epoxide is of the same absolute configuration as the highly tumorigenic isomers of the BP and chrysene bay region diol epoxides. The bay region diol epoxides of BA are also mutagenic in bacterial strains and in V79-6 Chinese hamster lung cells (*23*−*25*).

The oligodeoxynucleotide d(CGGACAAGAAG)·d(CTTCTTGTCCG) provides a model (*26*) (Chart 1) to examine the solution conformations of PAH adducts located site specifically at adenine N^6 in duplex DNA. The *ras*61 oligodeoxynucleotide facilitates investigation as to how DNA sequence and PAH ring structure each modulate adduct conformation in solution. The development of a nonbiomimetic synthesis enabled large-scale production of site-specific PAH adducts in the *ras*6 oligodeoxynucleotide while eliminating problems in controlling the regioselectivity of adduction (*26*−*30*). This oligodeoxynucleotide contains the codon 61 sequence for the human N-*ras* protooncogene (underlined). Mutations in codon 61 are linked to oncogene activation.

We examined a series of site-specific adenine N^6 PAH adducts in the *ras*61 oligodeoxynucleotide (*31*−*35*). These studies, as well as the work of others (*36*−*43*) reveal that a combination of factors interact to control the three-dimensional structure of adenine N^6 PAH adducts. These include stereochemistry at the benzylic carbon of the PAH, the arrangement of the PAH rings, and the DNA sequence. Sequence effects in the *ras*61 oligodeoxynucleotide were probed using the bay region benzo[*a*]pyrene SRSR (61,2) and SRSR (61,3) adducts. Those results revealed a single conformation for the BP SRSR (61,2) adduct but two conformations in rapid equilibrium for the BP SRSR (61,3) adduct (*34*, *44*). The sequence-specific structural differences were mirrored by differences in adduct processing as measured by site-specific mutagenesis. The BP SRSR (61,2) adduct showed low levels of A→G mutations, while the BP SRSR (61,3) adduct showed similar levels of two mutations, A→G and A→T (*45*). Subsequent site-specific mutagenesis experiments showed that the BA RSRS (61,2) adduct also induced A→G transitions, similar to the adenyl N^6 BP SRSR (61,2) adduct of corresponding stereochemistry (*46*), but with increased frequency.

The work presented here focuses on the solution structure of the BA RSRS (61,3) adduct (Chart 1). The structure is compared to the bay region BA RSRS (61,2) adduct, in which the lesion was located at position X^6 in the same oligodeoxynucleotide. The structural refinement for the BA RSRS (61,3) adduct reveals that the BA moiety intercalates above the 5′-face of the modified base pair from the major groove. Two sequence effects are noted, when the BA RSRS (61,3) adduct is compared with the BA RSRS (61,2) adduct (*33*). First, the PAH moiety stacks with the adenine base at A^6. Second, the deoxyribose sugar at A^6 shifts to an approximately equal blend of C2′-endo and C3′-endo conformations in rapid exchange. This is similar to the bay region benzo[*a*]pyrene BP SRSR (61,3) lesion (*34*) and may represent a sequence effect common to PAH adducts located at the (61,3) site of the *ras*61 oligodeoxynucleotide. For the BP SRSR (61,3) adduct, the shift in deoxyribose pseudorotation from C2′-endo to C3′-endo at A^6 was reflected in distinct base pairing geometries at the adduct site X^7·T^{16}. It cannot be discerned whether this is also the case for the BA RSRS (61,3) adduct. However, the structural results do suggest that, like the BP SRSR (61,3) adduct, the BA RSRS (61,3) adduct may induce multiple types of mutations in site-specific mutagenesis experiments.

MATERIALS AND METHODS

Materials. The oligodeoxynucleotide 5′-d(CTTCTTGTCCG)-3′ was purchased from the Midland Certified Reagent Co. (Midland, TX). The modified oligodeoxynucleotide 5′-d(CGGACAXGAAG)-3′ (Chart 1) was synthesized through a procedure in which (±)-amino triol derived from (±)-4β,3α-dihydroxy-2α,1α-epoxy-1,2,3,4-tetrahydrobenz[*a*]anthracene [(±)-DE2] was reacted with an oligodeoxynucleotide containing 6-fluoroadenosine at position X^7 (*26*, *28*, *29*). The (1*R*,2*S*,3*R*,4*S*)-*N*^{6}-[1-(1,2,3,4-tetrahydro-2,3,4-trihydroxybenz[*a*]anthracenyl)]-2′-deoxyadenosyl-modified oligodeoxynucleotide was purified from the reaction mixture by HPLC using a reverse-phase semipreparative column (PRP-1; Hamilton Co., Reno, NV) equilibrated with 10 mM ethylenediamineacetate (pH 7.0). The oligodeoxynucleotide was eluted with a gradient from 0 to 20% acetonitrile in 20 min. It was identified using multiple methods, including circular dichroism spectroscopy, enzymatic digestion, and mass spectroscopy. The DNA was lyophilized and desalted on Sephadex G-25 (Amersham-Pharmacia, Inc., Piscataway, NJ).

NMR Samples. The oligodeoxynucleotide concentrations were determined from extinction coefficients of 1.09×10^5 $M^{-1}\cdot cm^{-1}$ for modified and 9.24×10^4 $M^{-1}\cdot cm^{-1}$ for the complementary strands, at 260 nm (*47*). The complementary oligodeoxynucleotides were mixed at a 1:1 molar ratio in 0.1 M NaCl, 10 mM NaH_2PO_4, and 50 μM Na_2EDTA at pH 7. The mixture was heated to 90 °C for 5 min and was cooled to room temperature. DNA grade Bio-Gel hydroxylapatite

(Bio-Rad Laboratories, Hercules, CA) (15 cm × 3.0 cm), eluted with a gradient from 10 to 200 mM NaH_2PO_4 (pH 7.0), was used for the separation of double- from single-stranded oligodeoxynucleotides. The duplex was lyophilized and dissolved in 0.5 mL of H_2O and desalted on Sephadex G-25 (70 × 1.5 cm). The sample was lyophilized and redissolved in 0.5 mL of NMR buffer containing 0.1 M NaCl, 10 mM NaH_2PO_4, and 50 μM Na_2EDTA at pH 7.0. The solution was lyophilized and exchanged three times with 99.96% D_2O. The strand concentrations of the samples were approximately 1.8 mM. The samples used for examining nonexchangeable protons were dissolved in 99.996% D_2O buffer. The samples used for the examination of the exchangeable protons were in buffer solution containing 9:1 H_2O:D_2O.

UV Melting. The experiments were carried out on a Cary 4E spectrophotometer (Varian Associates, Palo Alto, CA). The buffer was 10 mM sodium phosphate, 0.05 mM Na_2-EDTA, and 1 M NaCl at pH 7.0. The buffer solution was degassed prior to the experiment. The concentrations were adjusted to 4.8×10^{-6} M in a 1 cm cuvette. The temperature was increased at a rate of 0.5 °C/min from 2 to 90 °C. Absorbance was measured at 260 nm. The melting temperatures of the native and modified oligodeoxynucleotides were calculated by determining the midpoints of the melting curves from the first-order derivatives.

NMR. Experiments were performed at ^{1}H frequencies of 750.13 and 500.13 MHz. To examine exchangeable protons, phase-sensitive NOESY experiments were carried out in 9:1 H_2O:D_2O buffer at a ^{1}H frequency of 500.13 MHz. The watergate pulse sequence suppressed the water signal (*48*). The spectra were recorded at 5 °C with a mixing time of 250 ms. The phase-sensitive NOESY spectra used in the nonexchangeable proton resonance assignments were recorded at 15 °C using TPPI quadrature detection. The mixing time was 250 ms. To derive the distance restraints from NOESY experiments, three spectra were recorded consecutively at mixing times of 100, 150, and 250 ms, respectively. In these experiments, the data were recorded with 1024 real data in the t_1 dimension and 2048 real data in the t_2 dimension. The relaxation delay was 2 s. The data were processed using FELIX (v. 97.0, Molecular Simulations, Inc., San Diego, CA) on Silicon Graphics (Mountain View, CA) Octane workstations. The data in the t_1 dimension were zero-filled to give a matrix of 2K × 2K real points. A skewed sine-bell-square apodization function with a 90° phase shift was used in both dimensions.

Generation of Restraints. Footprints were drawn around the NOE cross-peaks for the NOESY spectrum measured at a mixing time of 250 ms to define the size and shape of the individual cross-peaks using FELIX. The same set of footprints was applied to spectra measured at other mixing times. Cross-peak intensities were determined by volume integration of the areas under the footprints. The intensities were combined as necessary with intensities generated from complete relaxation matrix analysis of a starting DNA structure to generate a hybrid intensity matrix (*49*). MARDIGRAS (v. 3.0) (*50*, *51*) refined the hybrid matrix by iteration to optimize the agreement with experimental NOE intensities. The molecular motion was assumed isotropic. Calculations, generally requiring two to five cycles, were performed using DNA starting models generated by INSIGHTII (v. 97.0), the three mixing time NOE experiments, with four τ_c values (2, 3, 4, and 5 ns). The resulting sets of distances were averaged to give the experimental NOE restraints used in subsequent molecular dynamics calculations (*52*). For partially overlapped cross-peaks, lower or upper error bounds on the resulting distances were increased. The distance restraints were divided into five classes on the basis of the confidence factor obtained from MARDIGRAS.

Additional restraints were included. The deoxyribose DQF-COSY data for bases except A^6 and T^{16} were consistent with the C2′-endo sugar ring conformation (*53*). Therefore, except A^6 and T^{16}, the deoxyribose rings were restrained to the C2′-endo conformation. At A^6, COSY data suggested approximately equal populations of the C2′-endo and C3′-endo conformations. Therefore, two sets of calculations were run, one in which A^6 was restrained in the C2′-endo conformation and one in which A^6 was restrained in the C3′-endo conformation. There were no unusually shifted ^{31}P resonances in the duplex. This indicated that the phosphodiester backbone geometry was similar to that for B-DNA (*45*). Therefore, the backbone torsion angles ϵ and ζ were restrained to 165° ± 35° and 245° ± 35° (*54*). Watson−Crick hydrogen-bonding restraints were used, except for base pair A^6•T^{17}. The restraints were consistent with crystallographic data (*55*) and similar to those previously used in structural determination of oligodeoxynucleotides (*56*) except at base pair X^7•T^{16} (*57*). The T^{16} imino proton resonance was weak. Accordingly, an increased upper distance bound for the hydrogen-bonding restraint was used at this position.

Restrained Molecular Dynamics. Calculations were performed using X-PLOR (*58*) (v. 3.85). The force field was derived from CHARMM (*59*) and adapted for restrained MD calculations of nucleic acids. The approach utilized methodology described by Tinoco, Jr., and co-workers (*60*, *61*) and further developed by Allain and Varani (*62*, *63*). In the first stage of refinement, NOE and hydrogen-bonding distance restraints (except at the A^6•T^{17} base pair) only were utilized to determine the "global fold" of the oligodeoxynucleotide (*60*, *61*, *63*). Beginning with fifty independent structures having random torsion angles generated using X-PLOR by radomization of the α, β, γ, ϵ, and ζ angles (*53*), 10 "converged" structures were obtained. During the initial and global fold stage, all electrostatic interactions were turned off. The repulsive van der Waals potential was used. Experimental NOE and hydrogen bond distance restraints were used.

Subsequently, the "globally folded" intermediate structures were subjected to a refinement stage of restrained molecular dynamics utilizing a simulated annealing protocol that included NOE, torsion angle restraints, and empirical restraints. The empirical energy function (*59*) consisted of terms that could be individually manipulated for bonds, bond angles, torsion angles, tetrahedral and planar geometry, hydrogen bonding, and nonbonded interactions including van der Waals and electrostatic forces. It treated hydrogens explicitly. The van der Waals energy term used the Lennard-Jones potential energy function. The electrostatic term used the Coulomb function, based on a full set of partial charges (−1/residue) and a distance-dependent dielectric constant of 4*r*. The nonbonded pair list was updated if any atom moved more than 0.5 Å, and the cutoff radius for nonbonded interactions was 11 Å. Calculations were performed in vacuo

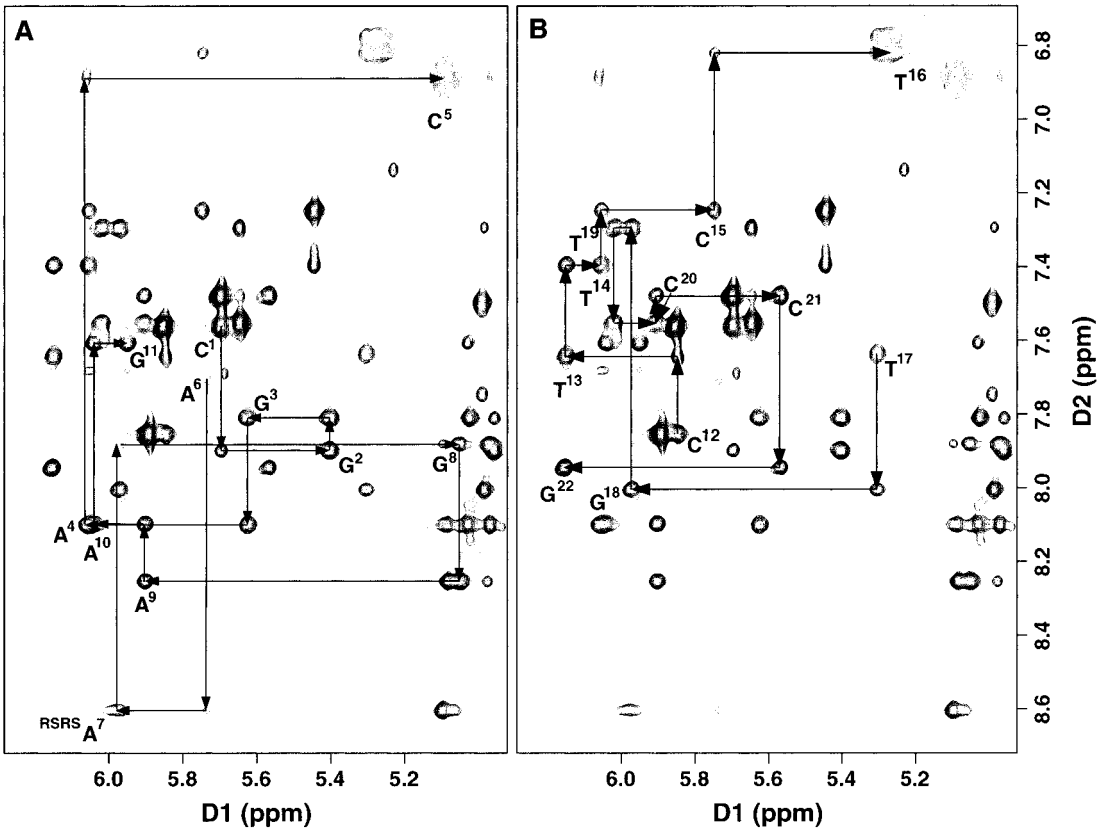

FIGURE 1: Expanded plots from the aromatic−anomeric region of the 750.13 MHz NOESY spectrum at 15 °C using a 250 ms mixing time. Sequential NOE connectivities for (A) the modified strand and (B) the complementary strand.

without explicit counterions. Calculations were initiated by coupling to a heating bath, with a target temperature of 1500 K. The force constants were 10 kcal mol^{-1} Å^{-2} for empirical hydrogen bonding, 20 kcal mol^{-1} Å^{-2} for torsion angle restraints, and 50, 45, 40, 35, and 30 kcal mol^{-1}Å^{-2} for the five classes of NOE restraints. The target temperature was reached in 5 ps and was maintained for 15 ps. The molecules were cooled to 300 K over 5 ps and maintained at that temperature for 25 ps of equilibrium dynamics. The force constants for the five classes of NOE restraints were scaled up for 3−5 ps during the heating period to 150, 130, 100, 100, and 100 kcal mol^{-1} Å^2 in the order of confidence factor. These weights were maintained during the reminder of the heating period and for the first 5 ps of the equilibrium dynamics period. They were then scaled down to 50, 45, 40, 35, and 30 kcal mol^{-1}Å^{-2} in the order of confidence factor. The torsion angle and base pair distance force constants were scaled up to 100 kcal mol^{-1} Å^{-2} during the same period as for the NOE restraints. They were scaled back to 20 and 10 kcal mol^{-1} Å^{-2}, also at the same time as the NOE restraints. Coordinate sets were archived every 0.1 ps, and 49 structures from the last 10 ps were averaged. These average rMD structures were subjected to 1100 iterations of conjugate gradient energy minimization to obtain the final structures. Final structures were analyzed using X-PLOR to measure rmsd between an average structure and the converged structures. Back-calculation of theoretical NMR intensities from the emergent structures was performed using CORMA (v. 4.0) (*49*). The structures were analyzed using DIALS AND WINDOWS 1.0, and structural parameters such as rise, buckle, and propeller twist were calculated (*64*).

RESULTS

Thermal Stability. The thermal stability of the BA RSRS (61,3) adduct was examined by UV melting studies that compared it with the unadducted *ras*61 sequence. The measured T_m was 45 °C. This adduct destabilized the duplex, as indicated by a 9 °C reduction in T_m as compared to the unmodified duplex. In comparison, the T_m of the corresponding BA RSRS (61,2) adduct, obtained under identical conditions, was 44 °C, a 10 °C reduction in T_m as compared to the unmodified duplex. Thus, the BA RSRS (61,3) adduct caused destabilization of the DNA duplex similar to that of the BA RSRS (61,2) adduct. The thermodynamic stability of the BA RSRS (61,3) adduct was also compared to that of the previously examined benzo[*a*]pyrene SRSR(61,3) adduct having corresponding stereochemistry. The latter adduct had given a 13 °C reduction in T_m as compared to the unmodified *ras*61 oligodeoxynucleotide. A series of ^{1}H spectra obtained from 10 to 35 °C indicated 15 °C to be the optimal temperature for NMR spectroscopy. At this temperature, the duplex was intact and the ^{1}H resonances were the sharpest and best resolved.

^{1}H Resonance Assignments. (a) Nonexchangeable Protons. The sequential NOEs between the aromatic and anomeric protons of the BA RSRS (61,3) adduct are displayed in Figure 1. Except at and adjacent to the lesion site, the spectrum was similar to that of the unmodified *ras*61 oligomer (*65*). For the modified strand, a break in the sequential connectivity was observed between C^5 H1′ and A^6 H8. A weaker than anticipated NOE connectivity for a B-DNA base step was observed between A^6 H1′ and A^6 H8 and between A^7 H1′ and G^8 H8. The A^6 H8 resonance was

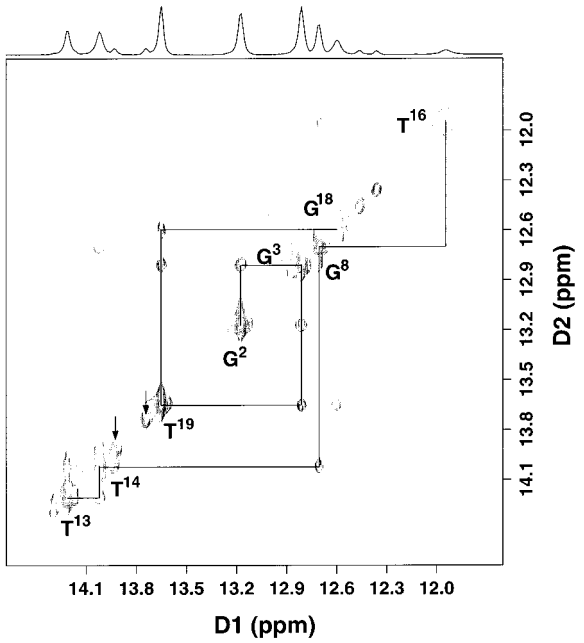

FIGURE 2: Expanded plot showing sequential NOE connectivities for the imino protons of base pairs G^2•C^{21}→A^{10}•T^{13}. The labels represent the imino proton of the designated base. Also shown is a 1D projection of the imino proton resonances. The 500.13 MHz NOESY spectrum was collected at 250 ms mixing time and 5 °C.

broad. In the complementary strand, the connectivity between T^{16} H1′ and T^{17} H6 was interrupted. The remainder of the sequential NOEs for the complementary strand appeared consistent with a B-DNA-like structure. The assignments of the sugar protons except H5′ and H5″ were determined from TOCSY and DQF-COSY spectra. No sequential NOEs were observed between C^5 H2″ and A^6 H8 and between A^6 H2″ and A^7 H8. The chemical shifts of the nonexchangeable protons are listed in Table S1 in the Supporting Information.

(b) Exchangeable Protons. Assignment of the imino protons was made from NOE connectivities between adjacent base pairs and connectivities to the base-paired amino protons (*66*). An expanded region showing cross-peaks between the imino protons is given in Figure 2. Sequential assignments of the imino protons from base pairs G^2•C^{21}→C^5•G^{18} and A^7•T^{16}→A^{10}•T^{13} were obtained unequivocally. An upfield-shifted and broadened resonance at 11.95 ppm had a weak connectivity to G^8 N1H. This was assigned to T^{16} N3H. The T^{17} N3H proton was exchange broadened but tentatively assigned at 12.4 ppm from a very weak cross-peak with G^{18} N1H. This implied disruption of Watson−Crick hydrogen bonding at A^6•T^{17}. No NOE connectivity was observed between T^{16} N3H and T^{17} N3H. Four minor resonances that could not be identified were observed. A minor second set of cross-peaks was observed for base pairs A^4•T^{19}, A^9•T^{14}, and A^{10}•T^{13}. This was unusual because none of these base pairs were proximal to the BA adduct. With the exception of the 5′-terminal nucleotides C^1 and C^{12}, distinctive amino proton resonances were observed for each cytosine. Unusual shifts were not observed for the cytosine amino protons. The chemical shifts of the exchangeable protons are listed in Table S2 of the Supporting Information.

(c) Benz[a]anthracene Protons. An expanded region of the NOESY spectrum used for the assignment of BA aromatic protons is shown in Figure 3. The numbering scheme for the BA protons is shown in Chart 1. The aromatic resonances were found in two clusters. The downfield cluster, in the chemical shift range 7.5−7.8 ppm, contained the H5, H6, and H7 resonances, whereas the upfield cluster, in the chemical shift range 6.4−6.8 ppm, contained the H8, H9,

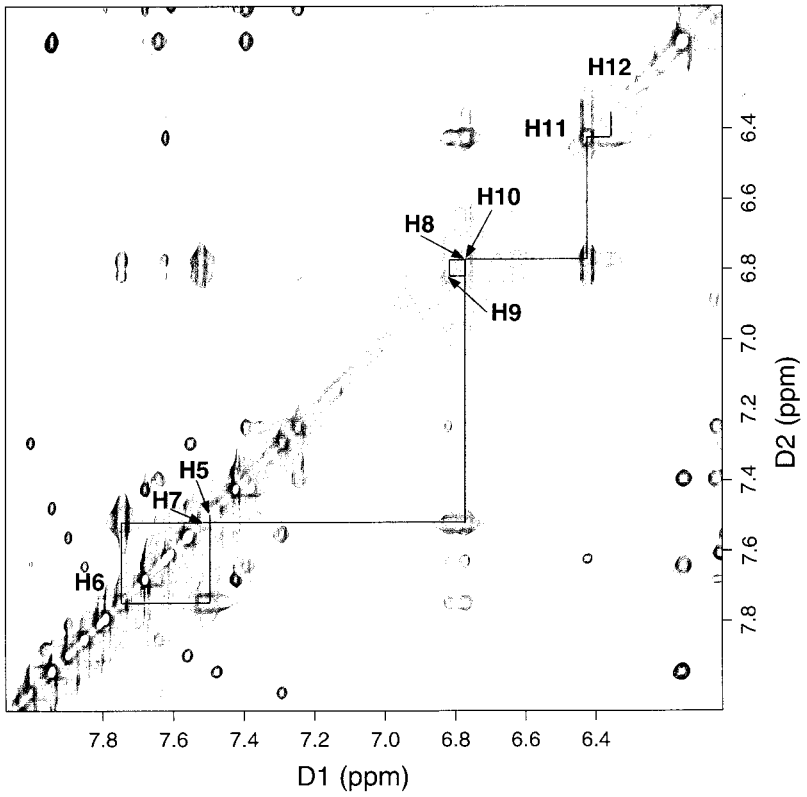

FIGURE 3: Expanded 750.13 MHz NOESY spectrum at 250 ms mixing time showing the assignments for the aromatic protons of BA. The experiment was at 15 °C.

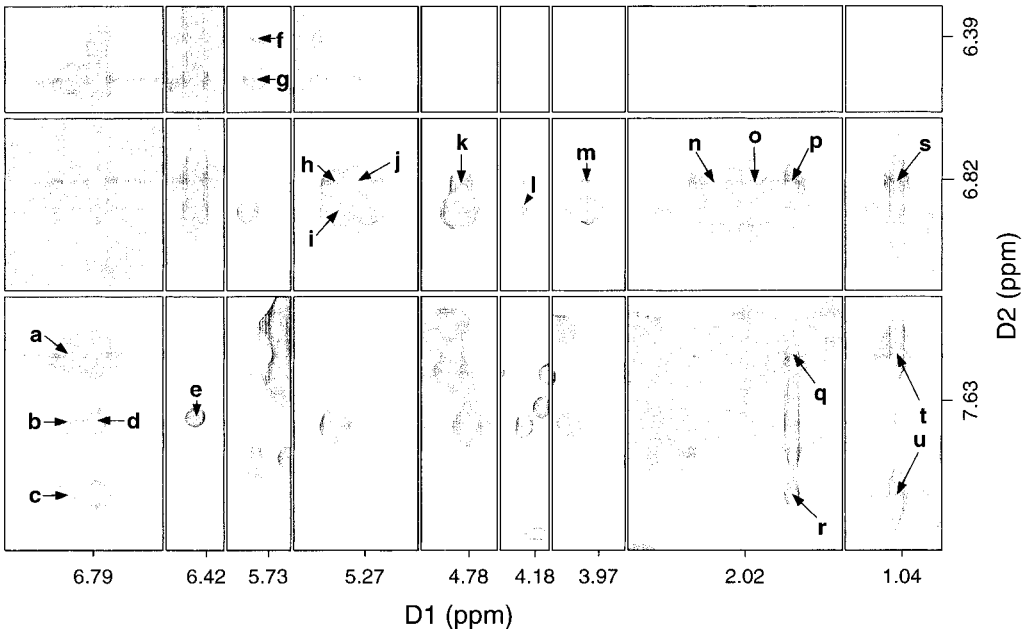

FIGURE 4: Tile plot showing NOE cross-peaks between nonexchangeable protons of DNA and BA protons: a, T^{16} H6→BA H7; b, T^{17} H6→BA H9; c, T^{16} H6→BA H6; d, T^{17} H6→BA H8; e, A^7 H2→BA H11; f, g, A^6 H1′→BA H12, H11; h, i, T^{17} H1′→BA H8, H9; j, T^{16} H1′→BA H10; k, T^{16} H3′→BA H8; l, T^{17} H4′→BA H9; m, T^{16} H4′→BA H8; n, o, T^{16} H2″, H2′→BA H8; p−r, T^{17} CH_3→BA H8, H7, H6; s−u, T^{16} CH_3→BA H8, H7, H6.

H10, H11, and H12 resonances. The distribution of these aromatic protons over the 1.3 ppm range of their chemical shifts was reminiscent of the anthracenyl protons of the BA RSRS (61,2) adduct in which the BA moiety was found to be intercalated (*29*). The aliphatic ring resonances H1 and H4 were assigned from their connectivities to BA aromatic protons, H11, H12 and H5, H6. The chemical shifts of the BA resonances are listed in Table S3 of the Supporting Information.

Benz[a]anthracene−DNA NOEs. There were 22 NOEs between the BA and DNA protons. All involved the modified base pair X^7•T^{16} and its 5′-neighbor A^6•T^{17} (Figure 4). The BA aromatic protons H6 and H7, located on the same face of the BA moiety, exhibited moderate to strong interstrand cross-peaks to T^{16} CH_3 and H6 and to T^{17} CH_3. Benz[*a*]-anthracene H8 showed interstrand cross-peaks to T^{16} H2′, H2″, H3′, and CH_3 and to T^{17} H1′, CH_3, and H6. Benz[*a*]-anthracene H9 also showed cross-peaks to T^{17} H1′ and H6. Cross-peaks were observed between BA H1, H11, and H12, located on the opposite face of the BA moiety from H5, H6, and H7, and A^6 H1′ and H3′. A cross-peak was also observed between the BA H11 and the exchangeable proton T^{16} N3H.

Sugar Pucker. Sugar puckering was assessed from DQF-COSY data. The deoxyribose sugars showed COSY cross-peaks that were consistent with the C2′-endo conformation characteristic of the B-DNA family (*53*), with one exception. The A^6 H1′−H2″ cross-peak pattern was altered as previously observed for the A^6 H1′−H2″ cross-peak in the benzo-[*a*]pyrene SRSR (61,3) adduct (*34*). This suggested that, similar to the benzo[*a*]pyrene adduct, the A^6 deoxyribose sugar conformation had a greater contribution from the C3′-endo conformation. The observation that there were no unusually shifted ^{31}P resonances indicated that the backbone geometry was similar to that for B-DNA (*45*).

Chemical Shift Perturbations. The chemical shifts of the nonexchangeable and exchangeable protons, compared to the unmodified *ras*61 sequence, are shown in Figure 5. For the imino protons, the greatest upfield shift of 2.1 ppm was observed for T^{16} N3H, the imino proton of the adducted base pair. For the base protons, an upfield chemical shift of 0.6 ppm was observed for T^{16} CH_3 and H6. A downfield chemical shift of 0.6 ppm was observed for A^7 H8. The deoxyribose protons around the adducted site exhibited chemical shift changes as well. At the site of the adduction, T^{16} H1′ experienced a 0.7 ppm upfield shift. A 0.5 ppm upfield shift was detected for T^{17} H1′. Long-range upfield chemical shift changes were also observed. C^5 H2′ and H2″ (two bases to the 5′-direction of the site of direction) experienced upfield shifts of 0.8−0.9 ppm. C^{15} H2′ and H2″ (3′-neighbor base to the site of direction) experienced upfield shifts of 0.6−0.7 ppm. Other smaller upfield shifts were observed for a number of protons near the adduction site.

Experimental Restraints. There were 485 experimental distance restraints derived from nonexchangeable ^{1}H NOEs by MARDIGRAS. These consisted of 306 intranucleotide restraints, 158 internucleotide restraints, and 21 BA−DNA restraints. The distribution of these restraints for each base is summarized in Figure S2 in the Supporting Information. The restraints were approximately evenly distributed along the length of the oligodeoxynucleotide. The smaller numbers of restraints for some nucleotides, e.g., A^6, were attributed to line broadening resulting in a loss of NOE cross-peaks. Another exception was C^5, which showed no internucleotide restraints with A^6. The restraints also included 100 sugar pucker restraints and 40 backbone angle restraints, assigned from inspection of ^{1}H−^{1}H and ^{1}H−^{31}P *J*-couplings that indicated most base pairs and torsion angles consistent with the B-DNA family. Additionally, 20 empirical planarity restraints were utilized. A list of experimental distance restraints along with the upper and lower bounds is shown in Table S4 of the Supporting Information.

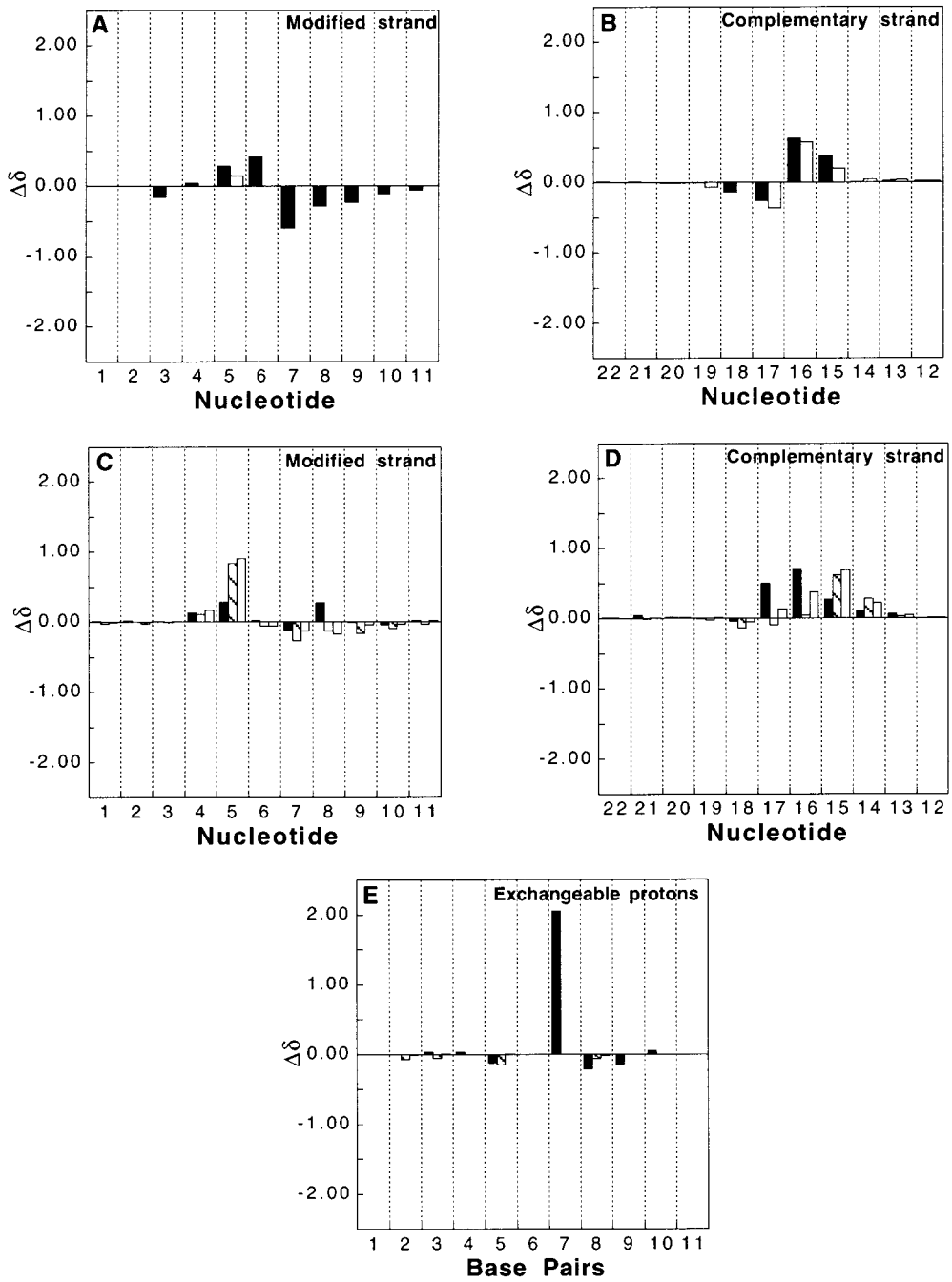

FIGURE 5: Chemical shift changes of selected protons relative to the unmodified oligodeoxynucleotide duplex. Panels A and B: Major groove protons in the modified and complementary strands, respectively. Bars: solid, G/A H8 or C/T H6; open, C H5 or T CH_3. Panels C and D: Minor groove protons in the modified and complementary strands, respectively. Bars: solid, H1′; crosshatched, H2′; open, H2″. Panel E: Exchangeable protons. Bars: solid, G N1H or T N3H; crosshatched, C N^4H(a); open, C N^4H(b). $\Delta\delta = [\delta_{\text{unmodified oligodeoxynucleotide}} - \delta_{\text{modified oligodeoxynucleotide}}]$ (ppm).

Structural Refinement. Because the COSY data suggested that the deoxribose ring of nucleotide A^6 could exist in either the C2′-endo or C3′-endo conformations, separate sets of molecular dynamics calculations were run, in which A^6 was restrained either as C2′-endo or as C3′-endo. An additional set of calculations was performed, with no pseudorotation restraint at A^6. Convergence was evaluated using energy, energy-ordered rmsd profiles (*62*, *67*) and R_1^x factor. The results of these separate calculations for different conformations of sugar A^6 showed that the differences in rmsd, energies, and R_1^x factors were similar to the differences within each set of calculations. For example, the rmsd between one C2′-endo structure and one C3′-endo structure was the same as between two C2′-endo structures. At the adducted pair, shifting the deoxyribose sugar at A^6 from the C2′-endo conformation to the C3′-endo conformation did not result in a calculated change in base pair geometry at the lesion site. In summary, the calculated differences in structure depending upon whether A^6 was in the C2′-endo or C3′-endo conformation were judged to be insignificant. Therefore, it was decided to work with a single average structure, representing the ensemble of C2′-endo and C3′-endo conformations at A^6. The total energies and NOE restraints violation energies for the averaged structures were lower than 3 and 0.04 kcal/mol, respectively. The maximum pairwise rmsd for the converged structures was 1.05 Å. Theoretical

Table 1: Analysis of the MD-Generated Structures of the BA RSRS (61,3) Adduct

NMR restraints	
total no. of distance restraints	485
interresidue distance restraints	158
intraresidue distance restraints	306
DNA−BA distance restraints	21
empirical restraints	
H-bonding restraints	26
dihedral planarity restraints	20
sugar pucker restraints	100
backbone torsion angle restraints	40
structural statistics	
NMR *R*-factor $(R_1^x)^{a,b,c}$	
⟨rMDRi⟩	0.0842 ± 0.0008
rmsd of NOE violations (Å)	0.037 ± 0.006
no. of NOE violations >0.2 Å	3 ± 2
in entire duplex	
rmsd from ideal geometry	
bond length (Å)	0.02435 ± 0.00002
bond angle (deg)	1.950 ± 0.003
improper angle (deg)	0.39 ± 0.03
pairwise rmsd (Å) over all atoms	
⟨rMDRi⟩ vs ⟨rMDav⟩	0.71 ± 0.15

[a] Only the inner nine base pairs were used in the calculations, to exclude end effects. The mixing time was 250 ms. All values for R_1^x are $\times 10^2$. [b] $R_1^x = \sum|(a_o)_i^{1/6} - (a_c)_i^{1/6}|/\sum|(a_o)_i^{1/6}|$, where a_o and a_c are the intensities of observed (nonzero) and calculated NOE cross-peaks. [c] ⟨rMDRi⟩, 10 converged structures starting from random torsion angles; ⟨rMDav⟩ , average of 10 converged structures.

NOE intensities were calculated from complete relaxation matrix analysis for the refined structures. These were compared to the experimental intensities. This comparison yielded sixth root residuals (*49*) of approximately 9%, both for intranucleotide NOEs and for internucleotide NOEs (Table 1). Figure 6 details the R_1^x values as a function of nucleotide, in the adducted duplex, neglecting the terminal base pairs.

Figure 7 shows a stereoview of 10 structures emergent from the rMD calculations. The stick−ribbon model shown in Figure 8 represents one of the converged structures. The converged structures were right-handed duplexes, in which the BA moiety intercalated from the major groove between A^6•T^{17} and X^7•T^{16}. The saturated ring of BA was oriented in the major groove of the duplex, with the aromatic rings inserted into the duplex such that the terminal ring of BA threaded the duplex and faced toward the minor groove direction. The duplex suffered localized distortion at and immediately adjacent to the adduct site. This was indicated by the increased rise of 8.2 Å as compared to the value of 3.5 Å normally observed for B-DNA between base pairs A^6•T^{17} and X^7•T^{16}. These two base pairs also buckled in opposite directions away from the intercalated BA moiety. Changes of 46° and −40° in buckle were calculated for A^6•T^{17} and X^7•T^{16}, respectively. The calculated structures predicted that T^{16} was twisted out of plane, as indicated by a 33° change in propeller twist for X^7•T^{16}. The BA adduct was accommodated in the DNA duplex without helical bending. The distortion in the duplex was localized, such that base pairs removed from the adduct remained in a B-like conformation.

DISCUSSION

Our intent in solving the solution structure of the BA RSRS (61,3) adduct was to probe the role of DNA sequence

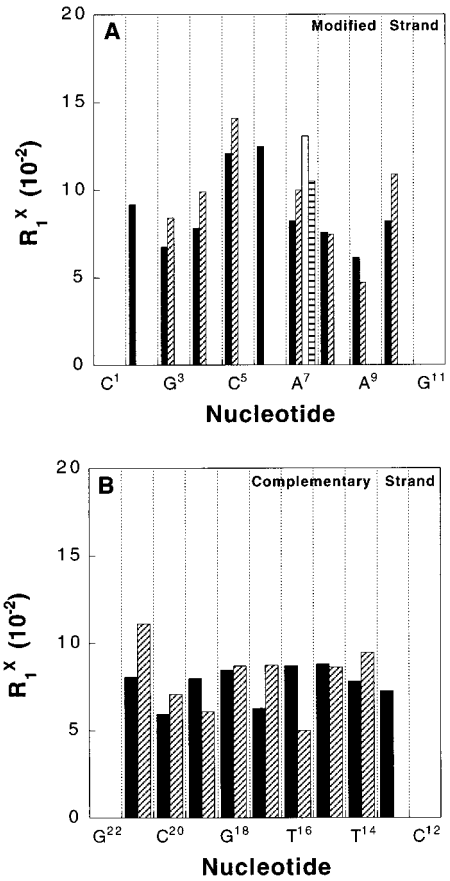

FIGURE 6: Bar diagrams showing the per-residue R_1^x values for the modified and complementary strands of the BA RSRS (61,3) adduct where the solid bars show the intraresidue R_1^x values, the crosshatch bars show the interresidue R_1^x values, the open bar shows the interstrand R_1^x values between X^7 and T^{16}, and the horizontal bar shows the interstrand R_1^x values between X^7 and T^{17}.

in modulating the conformation of this benz[*a*]anthracene adduct, via comparison with the previously examined BA RSRS (61,2) adduct (*33*). The latter was intercalated 5′ to the modified adenine. The notion that sequence effects might be operative came from structural (*34*, *44*) and site-specific mutagenesis studies (*45*) with the adenyl N^6 benzo[*a*]pyrene SRSR (61,2) and (61,3) adducts, located at the first and second adenines of the *ras*61 oligodeoxynucleotide. For those BP adducts, the adduct located at the (61,2) position exhibited a single conformation, whereas the adduct located at the (61,3) position was described as a mixture of two conformations in equilibrium (*27*, *28*). Those sequence-dependent differences in structure paralleled sequence-dependent differences in mutagenesis. The benzo[*a*]pyrene adduct at the (61,2) position yielded only A→G transitions in site-specific mutagenesis studies, whereas the same adduct at the (61,3) position yielded both A→G and A→T mutations (*45*).

Structure of the Benz[a]anthracene Lesion. Figure 8 shows the BA moiety intercalated from the major groove, above the 5′-face of the modified adenine. The present work extends the observed pattern for adenine N^6 PAH adducts, in which stereochemistry at benzylic carbon governs the intercalation direction of the PAH moiety. All *R* isomers examined to date intercalate toward the 5′-direction (*32*−*36*, *43*). Intercalation of the PAH moiety was consistent with the pattern of NOEs in the 5′-direction from the BA moiety to base pair A^6•T^{17} (Figure 9). The intercalated orientation of the BA ring

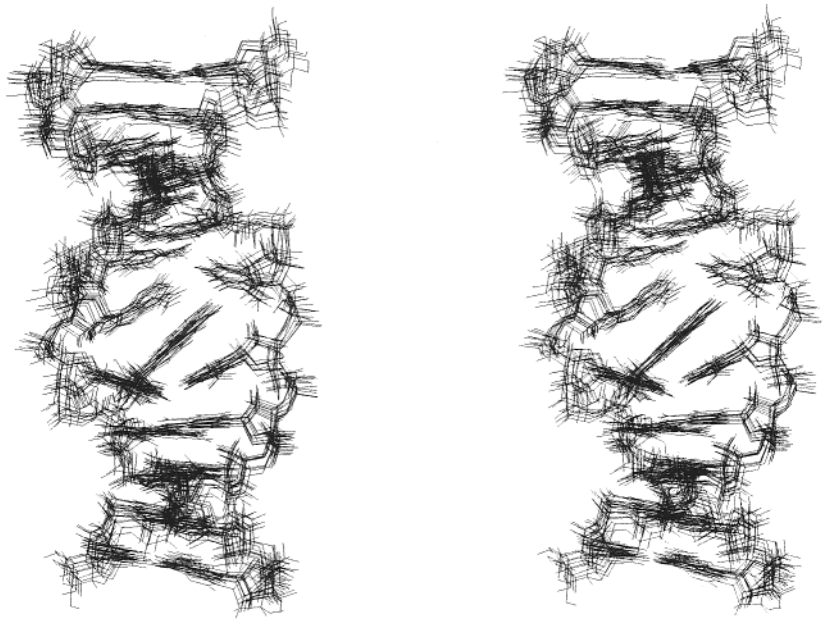

FIGURE 7: Stereoviews showing the comparisons of 10 superimposed structures emergent from the rMD calculations.

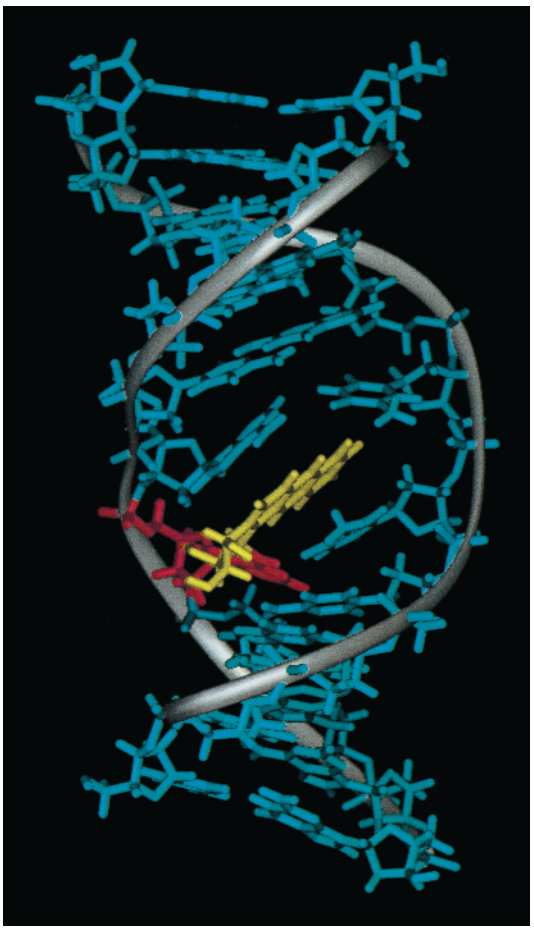

FIGURE 8: Stick−ribbon model representation of one converged structure. The BA moiety is colored in yellow.

resulted in distinctive NOEs between BA and DNA on the two faces of the BA ring. The BA aromatic protons H6 and H7 faced toward the major groove and exhibited moderate to strong NOEs to T^{16} and T^{17} CH_3. BA H8 showed NOEs to T^{16} H2′, H2″, and H3′. On the other hand, NOEs between BA H11, H12, and H1 and A^6 H1′ were explained by the location of these protons on the opposite face of the PAH ring. The normal NOE connectivity between the neighboring imino protons in base pairs A^6·T^{17} and X^7·T^{16} was missing, due to PAH intercalation. The over 1.3 ppm dispersion of the BA aromatic proton chemical shifts suggested that these protons existed in significantly different electronic environments, also consistent with intercalation. The increased rise of 8.2 Å, calculated between base pairs A^6·T^{17} and X^7·T^{16}, was consistent with intercalation. The BA aromatic protons H5, H6, and H7 were predicted to be less influenced by the ring currents of the adjacent nucleotide bases, whereas the protons H11 and H12 were positioned such that ring current shielding from A^6 was anticipated. This was consistent with the greater upfield shifts observed for the latter protons.

A notable feature was the prediction of a 5′-stacking interaction between the PAH rings of the benz[*a*]anthracenyl moiety and the A^6 purine, seen in Figure 10B. The rMD calculations predicted that the A^6 H8 proton should rotate into closer proximity to X^7 H8 because of this stacking interaction. It was not possible to discern from the NOESY data whether in fact this was the case. However, the formation of this stacking interaction was consistent with the interruption of sequential NOE connectivities between C^5 H1′ and A^6 H8 in Figure 1.

To accommodate intercalation of the BA adduct, base pair A^6·T^{17} underwent buckling, and disruption of Watson−Crick base pairing, relative to the unmodified *ras*61 oligomer. The difficulty in identifying the T^{17} imino resonance was consistent with enhanced solvent exchange, which would be predicted by the buckling of base pair A^6·T^{17}. The altered pattern of the A^6 H1′−H2" COSY cross-peak suggested an approximately equal blend of C2′-endo and C3′-endo conformations for the A^6 deoxyribose ring, similar to that observed for the corresponding BP SRSR (61,3) adduct (*34*).

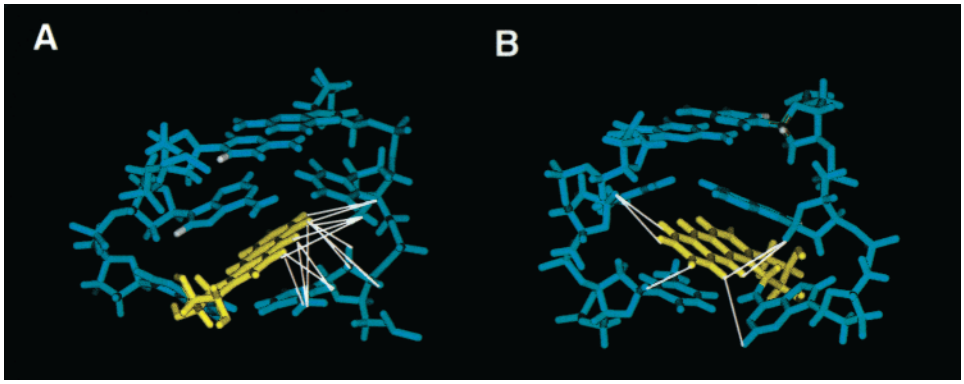

FIGURE 9: (A) Major groove view of the BA RSRS (61,3) adduct showing NOEs between BA protons H6, H7, H8, and H9 and the complementary strand of the DNA. Protons C^5 H6 and A6 H8 are indicated in white. The stacking of A^6 with the BA PAH moiety increased the distance between these two protons and between C^5 H1′ and A^6 H8, causing a break in NOE sequential connectivities. (B) Minor groove view of the BA RSRS (61,3) adduct showing NOEs between BA protons H8, H9, H10, H11, and H12 and the DNA. The NOEs are shown as white lines. The BA moiety is shown in yellow.

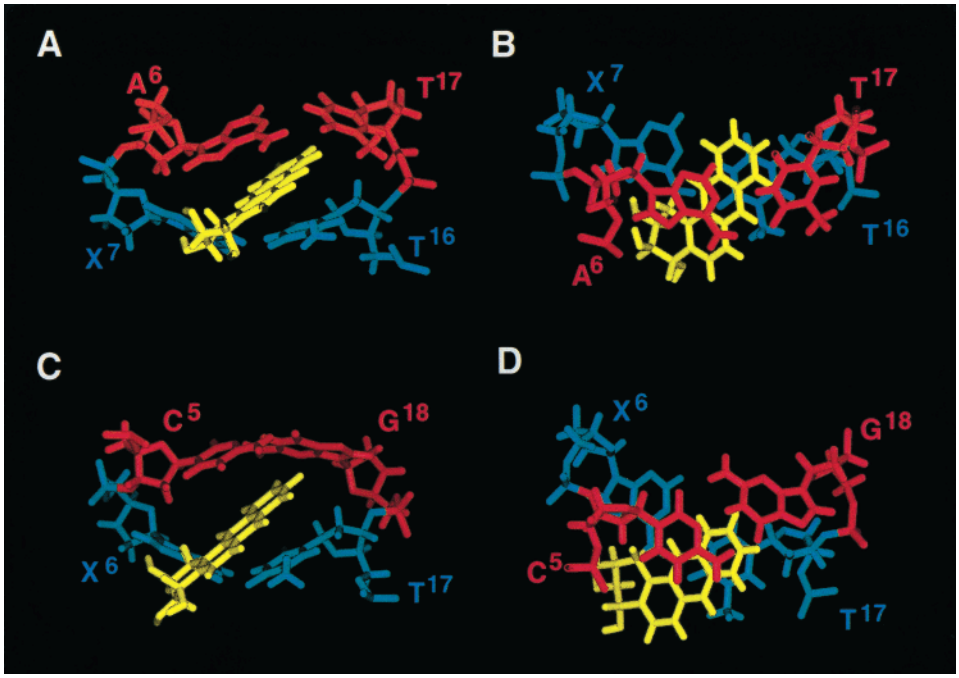

FIGURE 10: (A) View of base pairs A^6•T^{17} (red) and X^7•T^{16} (blue) in the BA RSRS (61,3) adduct. (B) Stacking pattern of base pair A^6•T^{17} (red) above X^7•T^{16} (blue) in the BA RSRS (61,3) adduct. (C) View of base pairs C^5•G^{18} (red) and X^6•T^{17} (blue) in the BA RSRS (61,2) adduct (*33*). (D) Stacking pattern of base pair C^5•G^{18} (red) above X^6•T^{17} (blue) in the BA RSRS (61,2) adduct (*33*). The BA moiety is colored in yellow.

This probably accounted for the upfield shifts of C^5 H2′ and H2″. The broadening observed for the C^5 H5 and C^5 H6 cross-peak in the NOE spectrum (Figure 1) was attributed to rapid pseudorotational interconversion at A^6.

Sequence Effect. A sequence effect was apparent for the BA RSRS (61,3) adduct as compared to the BA RSRS (61,2) adduct. For the latter, the intercalated BA moiety partially stacked with C^5 in the modified strand and with T^{17} in the complementary strand. Moreover, an adduct-induced alteration in pseudorotation at the 5′-neighbor base pair was not observed (*33*). This effect was similar to that observed for the corresponding BP adducts examined in the same oligodeoxynucleotide duplex (*34*, *44*). In both instances, the change to a 5′-neighbor A•T base pair from a 5′-neighbor C•G base pair altered potentially favorable stacking interactions between the PAH moiety and the 5′-neighbor purine base. At the (61,3) locus, the purine base of A^6•T^{17} was in the modified strand of the duplex, whereas at the (61,2) locus, the purine base of C^5•G^{18} was in the complementary strand.

The results of the BP study led to the prediction that shifting of the A^6 deoxyribose toward the normally disfavored C3′-endo conformation might enable improved stacking between the BP PAH moiety and the A^6 purine (*34*). Structural studies of the BA RSRS (61,2) adduct predicted that the more favorable arrangement of aromatic rings in the BA adduct should facilitate intercalation on the 5′-side of the modified deoxyadenosine (*33*). Thus, we predicted that, for the BA RSRS (61,3) adduct, stacking between A^6 and the BA PAH moiety might shift the deoxyribose pseudorotation for A^6 entirely toward the C3′-endo conformation (*34*). The present data suggest that this is not the case. The BA RSRS (61,3) adduct did stack with A^6, and the anthracenyl moiety was closer to the DNA helical axis as compared to the "quasi-intercalated" geometry of the corresponding

BP adduct. However, it did not increase the amount of C3′-endo conformation at A^6. We conclude that BP and BA adduct-induced shifts of the A^6 deoxyribose ring toward a blend of C2′-endo and C3′-endo conformations at the (61,3) locus of the *ras*61 oligodeoxynucleotide, as compared to the (61,2) locus, probably cannot be explained solely in terms of improved stacking between the PAH and the A^6 purine ring.

Comparison with the HPRT Oligodeoxynucleotide. The HPRT locus in Chinese hamster V-79 cells shows a "hot spot" for A→C mutations, following exposure to low levels of the (+)-(*R*,*S*,*S*,*R*) anti-trans stereoisomer of BPDE (*15*). It contains the same 5′-CAXG-3′ sequence (X indicates the hot spot for A→C mutations) as does the BA RSRS (61,3) adduct studied in this work. The BP SRSR adduct at the second adenine N^6 in the HPRT locus was examined by Volk et al., who reported evidence of syn−anti interconversion about the glycosyl bond at the modified deoxyadenosine (*68*). This was based upon the observation of unexpected cross-peaks in the 6.8−7.8 ppm region of the ^{1}H spectrum. These were assigned as exchange peaks from the modified deoxyadenosine H2 and H8 protons with a minor (∼5%) syn conformation.

In the present work, several unexpected cross-peaks between nonexchangeable protons were also observed, in the same spectral region as reported by Volk et al. (*68*). There were a number of observations that argued against the attribution of these to syn−anti interconversion at X^7 for the BA RSRS (61,3) adduct. The failure to observe additional exchange peaks, particularly involving ^{1}H resonances near base pair X^7•T^{16} or the BA PAH moiety, was inconsistent with syn−anti interconversion of the modified dA. Substantial chemical shift differences for a number of protons near the lesion site would have been predicted for such an interconversion. Moreover, the syn conformation of dA would have been predicted to result in an unusually intense NOE between X^6 H8 and X^6 H1′. This also was not observed. Thus, it was concluded that the BA RSRS (61,3) sample contained a minor species (<5%) in slow exchange with the predominant species. However, the identity of this minor species could not be discerned.

Biological Implications. For the BP SRSR (61,3) adduct, changing pseudorotation at A^6 from C2′-endo to C3′-endo was reflected in different base pairing geometry at X^7•T^{16} for the C3′-endo conformation as opposed to the C2′-endo conformation (*34*). This correlated with the observation that two types of mutations were observed when the BP lesion was placed at the (61,3) locus, A→G transitions and A→T transversions (*45*). In contrast, the BP lesion placed at the (61,2) locus existed in a single conformation (*34*) and caused only A→G transitions (*45*). The observation of a similar sequence-dependent effect on pseudorotation at base pair A^6•T^{17} for the BA RSRS (61,3) adduct examined in this work suggests that, like the BP SRSR (61,3) adduct, it may induce more than one type of mutation.

Whether the multiple conformations observed for the 5′-neighbor deoxyribose ring for these BP and BA adducts can account for multiple types of mutations at the (61,3) site in *ras* remains unclear. The energetic barrier between these two pseudorotation conformations of the deoxyribose ring is small in duplex DNA, as evidenced by rapid (NMR time scale) interconversion between them. It is difficult to understand why such conformational heterogeneity could account for multiple types of mutations, unless it was somehow amplified by protein−DNA interactions in a replication complex. The reported slow (NMR time scale) syn−anti interconversion of the BP adduct in the HPRT sequence (*68*) provides a potentially more attractive explanation for sequence-dependent mutagenesis results in the *ras*61 oligodeoxynucleotide. Yet, the syn conformation for BP reported in the HPRT sequence was present at only 5% (*68*), which would not account for the similar levels of both A→G and A→T mutations observed at position (61,3) in the *ras*61 sequence (*45*). On the other hand, the relative ratios of the syn vs the anti conformations at X^7 could differ in a replication complex, or the minor conformation could represent an unusually mutagenic species.

CONCLUSIONS

The structure of the bay region BA RSRS (61,3) adduct confirmed the role of DNA sequence in modulating DNA conformation. Two sequence effects were noted upon moving the BA adduct from the (61,2) position to the (61,3) position of the N-*ras* oligodeoxynucleotide. The first was the stacking interaction between the BA moiety and A^6. The second was a shift in the pseudorotation equilibrium at A^6 to an approximately equal blend of C2′-endo and C3′-endo conformations, in rapid exchange. The shift in pseudorotation at A^6 was also observed for the bay region BP SRSR (61,3) adduct (*34*). It may represent a general pattern applicable to other PAHs in this sequence context. The origin of the increased C3′-endo population at A^6 and its relationship to mutagenesis remain to be explained fully. The results suggest the possibility that the BA RSRS (61,3) adduct, like the BP SRSR (61,3) adduct, will exhibit a more complex mutational spectrum as compared to the BA RSRS (61,2) lesion, which produced only A→G mutations (*70*).

ACKNOWLEDGMENT

We thank Mr. Markus Voehler for assistance with the collection of NMR data.

SUPPORTING INFORMATION AVAILABLE

Tables S1−S3, which detail the ^{1}H NMR chemical shift assignments; Table S4, which shows the experimental distances and classes of restraints; Figure S1, which shows atomic charges obtained for the RSRS (61,3) BA lesion; Figure S2, which shows distribution of experimental NOE restraints applied in the structural refinement. This material is available free of charge via the Internet at http://pubs.acs.org.

REFERENCES

1. Grimmer, G. (1979) in *Environmental Carcinogens—Selected Methods of Analysis III*, International Agency for Research on Cancer, Lyon, France.
2. International Agency for Research on Cancer (1983) in *Monograph on the Evaluation of Carcinogenic Risk of the Chemical to Man: Certain Polycyclic Aromatic Hydrocarbons and Heterocyclic Compounds*, Lyon, France.
3. Snook, M. E., Severson, R. F., Arrendale, R. F., Higman, H. C., and Chortyk, O. (1977) *Beitr. Tabakforsch. 9*, 79−101.
4. Pott, P. (1963) *Natl. Cancer Inst. Monogr. 10*, 7−13.
5. Yang, S. K. (1988) *Biochem. Pharmacol. 37*, 61−70.

6. Guengerich, F. P., and Shimada, T. (1991) *Chem. Res. Toxicol. 4*, 391−407.
7. Dipple, A., Moschel, R. C., and Bigger, C. A. H. (1984) in *Chemical Carcinogens* (Searle, C. E., Ed.) pp 41−163, American Cancer Society, Washington, DC.
8. Geacintov, N. E. (1985) in *Polycyclic Hydrocarbons and Carcinogenesis* (Harvey, R. G., Ed.) pp 107−124, ACS Symposium Series, American Chemical Society, Washington, DC.
9. Thakker, D. R., Yagi, H., Levin, W., Wood, A. W., Conney, A. H., and Jerina, D. M. (1985) in *Bioactivation of Foreign Compounds* (Anders, M. W., Ed.) pp 177−242, Academic Press, New York.
10. Jennette, K. W., Jeffery, A. M., Blobstein, S. H., Beland, F. A., Harvey, R. G., and Weinstein, I. B. (1977) *Biochemistry 16*, 932−938.
11. Osborne, M. R., Jacobs, S., Harvey, R. G., and Brookes, P. (1981) *Carcinogenesis 2*, 553−558.
12. Dipple, A., Pigott, M., Moschel, R. C., and Costantino, N. (1983) *Cancer Res. 43*, 4132−4135.
13. Vousden, K. H., Bos, J. L., Marshall, C. J., and Phillips, D. H. (1986) *Proc. Natl. Acad. Sci. U.S.A. 83*, 1222−1226.
14. Ralston, S. L., Seidel, A., Luch, A., Platt, K. L., and Baird, W. M. (1995) *Carcinogenesis 16*, 2899−2907.
15. Wei, S. J., Chang, R. L., Bhachech, N., Cui, X. X., Merkler, K. A., Wong, C. Q., Hennig, E., Yagi, H., Jerina, D. M., and Conney, A. H. (1993) *Cancer Res. 53*, 3294−3301.
16. Wei, S. J., Chang, R. L., Wong, C. Q., Bhachech, N., Cui, X. X., Hennig, E., Yagi, H., Sayer, J. M., Jerina, D. M., Preston, B. D., and Conney, A. H. (1991) *Proc. Natl. Acad. Sci. U.S.A. 88*, 11227−11230.
17. Harvey, R. G. (1982) *Am. Sci. 70*, 386-393.
18. Conney, A. H. (1982) *Cancer Res. 42*, 4875−4917.
19. Harvey, R. G. (1991) in *Polycyclic Aromatic Hydrocarbons: Chemistry and Carcinogeneicity*, Cambridge University Press, Cambridge.
20. Buening, M. K., Wislocki, P. G., Levin, W., Yagi, H., Thakker, D. R., Akagi, H., Jerina, D. M., and Conney, A. H. (1978) *Proc. Natl. Acad. Sci. U.S.A. 75*, 5358−5361.
21. Thakker, D. R., Levin, W., Yagi, H., Tada, M., Ryan, D. E., Thomas, P. E., Conney, A. H., and Jerina, D. M. (1982) *J. Biol. Chem. 257*, 5103−5110.
22. Levin, W., Chang, R. L., Wood, A. W., Yagi, H., Thakker, D. R., Jerina, D. M., and Conney, A. H. (1984) *Cancer Res. 44*, 929−933.
23. Slaga, T. J., Huberman, E., Selkirk, J. K., Harvey, R. G., and Bracken, W. M. (1978) *Cancer Res. 38*, 1699−1704.
24. Wood, A. W., Levin, W., Lu, A. Y., Ryan, D., West, S. B., Lehr, R. E., Schaefer-Ridder, M., Jerina, D. M., and Conney, A. H. (1976) *Biochem. Biophys. Res. Commun. 72*, 680−686.
25. Wood, A. W., Chang, R. L., Levin, W., Lehr, R. E., Schaefer-Ridder, M., Karle, J. M., Jerina, D. M., and Conney, A. H. (1977) *Proc. Natl. Acad. Sci. U.S.A. 74*, 2746−2750.
26. Kim, S. J., Jajoo, H. K., Kim, H.-Y., Zhou, L., Horton, P., Harris, C. M., and Harris, T. M. (1995) *Bioorg. Chem. 3*, 811−822.
27. Harris, T. M., Harris, C. M., Kim, S. J., Kim, H. Y., and Zhou, L. (1994) in *Polycyclic Aromatic Compounds* (Cavalieri, E., and Rogan, E., Eds.) pp 9−16, Harwood Academic Press, Philadelphia, PA.
28. Kim, S. J., Stone, M. P., Harris, C. M., and Harris, T. M. (1992) *J. Am. Chem. Soc. 114*, 5480−5481.
29. Kim, S. J., Harris, C. M., Koreeda, M., and Harris, T. M. (1991) *Tetrahedron Lett. 32*, 6073−6076.
30. Harris, C. M., Zhou, L., Strand, E. A., and Harris, T. M. (1991) *J. Am. Chem. Soc. 113*, 4328−4329.
31. Li, Z., Kim, H. Y., Tamura, P. J., Harris, C. M., Harris, T. M., and Stone, M. P. (1999) *Biochemistry 38*, 16045−16057.
32. Li, Z., Kim, H. Y., Tamura, P. J., Harris, C. M., Harris, T. M., and Stone, M. P. (1999) *Biochemistry 38*, 14820−14832.
33. Li, Z., Mao, H., Kim, H. Y., Tamura, P. J., Harris, C. M., Harris, T. M., and Stone, M. P. (1999) *Biochemistry 38*, 2969−2981.
34. Zegar, I. S., Chary, P., Jabil, R. J., Tamura, P. J., Johansen, T. N., Lloyd, R. S., Harris, C. M., Harris, T. M., and Stone, M. P. (1998) *Biochemistry 37*, 16516−16528.
35. Zegar, I. S., and Stone, M. P. (1996) *Chem. Res. Toxicol. 9*, 114−125.
36. Cosman, M., Fiala, R., Hingerty, B. E., Laryea, A., Lee, H., Harvey, R. G., Amin, S., Geacintov, N. E., Broyde, S., and Patel, D. (1993) *Biochemistry 32*, 2488−2497.
37. Tan, J., Geacintov, N. E., and Broyde, S. (2000) *J. Am. Chem. Soc. 122*, 3021−30320.
38. Cosman, M., Laryea, A., Fiala, R., Hingerty, B. E., Amin, S., Geacintov, N. E., Broyde, S., and Patel, D. J. (1995) *Biochemistry 34*, 1295−1307.
39. Geacintov, N. E., Cosman, M., Hingerty, B. E., Amin, S., Broyde, S., and Patel, D. J. (1997) *Chem. Res. Toxicol. 10*, 111−146.
40. Schwartz, J. L., Rice, J. S., Luxon, B. A., Sayer, J. M., Xie, G., Yeh, H. J., Liu, X., Jerina, D. M., and Gorenstein, D. G. (1997) *Biochemistry 36*, 11069−11076.
41. Yeh, H. J. C., Sayer, J. M., Liu, X., Altieri, A. S., Byrd, R. A., Lakshman, M. K., Yagi, H., Schurter, E. J., Gorenstein, D. G., and Jerina, D. M. (1995) *Biochemistry 34*, 13570−13581.
42. Schurter, E. J., Yeh, H. J. C., Sayer, J. M., Lakshman, M. K., Yagi, H., Jerina, D. M., and Gorenstein, D. G. (1995) *Biochemistry 34*, 1364−1375.
43. Schurter, E. J., Sayer, J. M., Oh-hara, T., Yeh, H. J. C., Yagi, H., Luxon, B. A., Jerina, D. M., and Gorenstein, D. G. (1995) *Biochemistry 34*, 9009−9020.
44. Zegar, I. S., Kim, S. J., Johansen, T. N., Horton, P., Harris, C. M., Harris, T. M., and Stone, M. P. (1996) *Biochemistry 35*, 6212−6224.
45. Chary, P., Latham, G. J., Robberson, D. L., Kim, S. J., Han, S., Harris, C. M., Harris, T. M., and Lloyd, R. S. (1995) *J. Biol. Chem. 270*, 4990−5000.
46. Millican, T. A., Mock, G. A., Chauncey, M. A., Patel, T. P., Eaton, M. A. W., Gunning, J., Cutbush, S. D., Neidle, S., and Mann, J. (1984) *Nucleic Acids Res. 12*, 7435−7453.
47. Borer, P. N. (1975) in *Handbook of Biochemistry and Molecular Biology*, CRC Press, Cleveland, OH.
48. Piotto, M., Saudek, V., and Sklenar, V. (1992) *J. Mol. Biol. 6*, 661−665.
49. Keepers, J. W., and James, T. L. (1984) *J. Magn. Reson. 57*, 404−426.
50. Borgias, B. A., and James, T. L. (1990) *J. Magn. Reson. 87*, 475−487.
51. Liu, H., Tonelli, M., and James, T. L. (1996) *J. Magn. Reson. B 111*, 85−89.
52. Schmitz, U., and James, T. L. (1995) *Methods Enzymol. 261*, 3−44.
53. Rinkel, L. J., and Altona, C.(1987) *J. Biomol. Struct. Dyn. 4*, 621−649.
54. Nikonowicz, E. P., and Gorenstein, D. G. (1990) *Biochemistry 29*, 8845−8858.
55. Saenger, W. (1984) in *Principles of Nucleic Acid Structure*, Springer, New York.
56. Weisz, K., Shafer, R. H., Egan, W., and James, T. L. (1994) *Biochemistry 33*, 354−366.
57. Tonelli, M., Ragg, E., Bianucci, A. M., Lesiak, K., and James, T. L. (1998) *Biochemistry 37*, 11745−11761.
58. Brunger, A. T. (1992) in *X-PLOR Version 3.1. A System for X-ray Crystallography and NMR*, Yale University Press, New Haven, CT.
59. Nilsson, L., Clore, G. M., Gronenborn, A. M., Brunger, A. T., and Karplus, M. (1986) *J. Mol. Biol. 188*, 455−475.
60. Wimberly, B., Varani, G., and Tinoco, I., Jr. (1993) *Biochemistry 32*, 1078−1087.
61. Wimberly, B. T. (1992) NMR derived structures of RNA loops: The conformation of eukaryotic 5S ribosomal loop E, Ph.D. Dissertation, University of California, Berkeley.
62. Allain, F. H., and Varani, G. (1997) *J. Mol. Biol. 267*, 338−351.
63. Allain, F. H., and Varani, G.(1995) *J. Mol. Biol. 250*, 333−353.

64. Ravishankar, G., Swaminathan, S., Beveridge, D. L., Lavery, R., and Sklenar, H. (1989) *J. Biomol. Struct. Dyn. 6*, 669−699.
65. Feng, B., and Stone, M. P. (1995) *Chem. Res. Toxicol. 8*, 821−832.
66. Boelens, R., Scheek, R. M., Dijkstra, K., and Kaptein, R. (1985) *J. Magn. Reson. 62*, 378−386.
67. Mauffret, O., Amir-Aslani, A., Maroun, R. G., Monnot, M., Lescot, E., and Fermandjian, S. (1998) *J. Mol. Biol. 283*, 643−655.
68. Volk, D. E., Rice, J. S., Luxon, B. A., Yeh, H. J. C., Liang, C., Xie, G., Sayer, J. M., Jerina, D. M., and Gorenstein, D. G. (2000) *Biochemistry 39*, 14040−14053.
69. Meadows, R., Post, C. B., Luxon, B. A., and Gorenstein, D. G. (1996) MORASS Program, University of Texas Medical Branch, Galveston, TX.
70. McNees, A. G., O'Donnell, M., Horton, P. H., Kim, H. Y., Kim, S. J., Harris, C. M., Harris, T. M., and Lloyd, R. S. (1997) *J. Biol. Chem. 272*, 33211−33219.

BI002785R